Results in Physics 6 (2016) 698–703

Contents lists available at ScienceDirect

Results in Physics

journal homepage: www.journals.elsevier.com/results-in-physics

Pulsed laser linewidth measurement using Fabry–Pérot scanning interferometer

Junwen Xue *, Wei Chen, Ying Pan, Jinqian Shi, Yujie Fang, Haijun Xie, Mingyuan Xie, Lu Sun, Binghua Su

Beijing Institute of Technology, Zhuhai, Key Laboratory of Photoelectric Imaging Technology and System (Zhuhai Branch) Ministry of Education of China, Collaborative Innovation Center of Photoelectric Information Technology and Application, 519088, China

ARTICLE INFO

Article history:
Received 4 July 2016
Received in revised form 26 August 2016
Accepted 6 October 2016
Available online 8 October 2016

Keywords:
Pulsed laser
Linewidth
Fabry–Pérot interferometer

ABSTRACT

We apply the Fabry–Pérot (FP) scanning interferometer, which is normally used for continuous wave (CW) laser linewidth measurement, for the measurement of pulsed laser linewidths. We analyze the response of the FP interferometer to continuous and pulsed lasers, also different detectors and suitable oscilloscope test parameters being selected for the measurement. For low-speed detectors, we set our oscilloscope to 1-MΩ impedance matching in the sampling mode. For high-speed detectors, we use the same oscilloscope test parameters or 50-Ω impedance matching with the peak-detection mode. With our setup, we achieve on-line linewidth measurement of a nanosecond pulsed laser for single-longitudinal and multi-longitudinal modes. Meanwhile, the linewidth measurement at different pulse repetition rates as low as 1 Hz is also demonstrated. The possibility of detecting the linewidth for pulse widths larger than 100 ps in the 1-μm band is discussed. The application range of the FP scanning interferometer is thus extended to the measurement of pulsed laser linewidths.

Introduction

The measurement of laser linewidth is integral to many applications in optical physics, metrology, and telecommunications among other research areas. In this context, five different techniques based on self-homodyning (SHO), self-heterodyning (SHE), Michelson interferometry (MI), Mach–Zehnder interferometry (MZI), and Fabry–Pérot interferometry (FP) have been used for laser linewidth measurement [1,2]. Among these, SHO and SHE provide the highest resolution (better than 1 kHz) with appropriate fiber lengths and Lorentzian line-shapes [3]. MI and MZI afford a resolution better than 30 kHz with careful adjustment, while the resolution of the standard FP interferometer is limited to 1 MHz [1]. However, the use of an optical fiber FP interferometer can improve the resolution to 4 kHz [4]. Further, the FP interferometer is the easiest to use among all the above mentioned instruments and approaches [1]. In general, FP interferometers used to measure laser linewidths are available in two forms: FP etalons and FP scanning interferometers [4–8]. The former is normally applied for pulsed laser linewidth measurements [9]. While the latter is generally used for continuous wave (CW) laser linewidth measurements [10]. Although researchers have used the latter to measure the pulsed laser linewidth [11–15], their studies have not been detailed.

In this background, in our study, we carry out a systematic measurement of the pulsed laser linewidth using an FP scanning interferometer. We analyze the response of the FP interferometer to continuous and pulsed lasers. Further, we also achieve on-line linewidth measurements of a nanosecond pulsed laser for the single-longitudinal mode and multiple-longitudinal modes using low- and high-speed detectors. Our approach enables linewidth measurements of pulses with repetition rates as low as 1 Hz. The possibility of detecting the linewidth for pulse widths larger than 100 ps in 1-μm band is discussed. To summarize, the application range of the FP scanning interferometer is extended to the measurement of pulsed laser linewidths.

Response of FP interferometer to CW and pulsed lasers

The basic principle of the FP interferometer is multi-beam interference. For an air gap structure, the factors of mirror surface distortion, mirror misalignment, scattering losses, and absorptions in the mirror coatings that affect the FP finesse are ignored [16,17]. The intensity reflectivity R of the two mirrors is assumed to be identical. The corresponding intensity transmission is $T = 1 - R$. When the incident direction of the laser is perpendicular to the mirrors, the normalized transmission intensity $Im(\phi)$ of the FP interferometer is a superposition of m-wave interference as [18]

* Corresponding author.
E-mail address: xuejunwen001@126.com (J. Xue).

http://dx.doi.org/10.1016/j.rinp.2016.10.004
2211-3797/

$$I_m(\phi) = \left|\sum_{n=0}^{m-1} TR^n e^{in\phi}\right|^2 = \left|T\frac{1-R^m e^{im\phi}}{1-Re^{i\phi}}\right|^2 \quad (1)$$

In Eq. (1), $\phi = 4\pi d/\lambda$ represents the adjacent beam phase difference, d the distance between the two mirrors, λ the wavelength in vacuum, and i the unit imaginary number.

For the superposition of infinite-beam interference, the normalized transmission intensity is given as [19]

$$I_\infty(\phi) = \left|\sum_{n=0}^{\infty} TR^n e^{in\phi}\right|^2 = \left|T\frac{1}{1-Re^{i\phi}}\right|^2 = \frac{[T/(1-R)]^2}{1+[4R/(1-R)^2]\sin^2(\phi/2)} \quad (2)$$

For a pulsed laser, upon ignoring the interference between pulses, we note that the superposition number is limited for a fixed pulse duration [18,20–22]. For the CW laser, upon ignoring the interference between wave trains, we note that superposition number is also limited by the coherence length. Therefore, the use of the Eq. (1) is more general, while Eq. (2) represents the ideal case.

When the intensity reflectivity is fixed, with increase in the superposition number, the peak transmittance increases to unity with an accompanying decrease in bandwidth, as shown in Fig. 1 (a). Further, for a fixed superposition number, with increase in intensity reflectivity, the peak transmittance and bandwidth decrease, as shown in Fig. 1(b).

The distance between the two mirrors can be varied by affixing a piezoelectric ceramic (PZT) with a suitable applied positive voltage to one mirror. In such a case, a half-wavelength distance change will lead to a free spectral range scanning, as shown in Fig. 2. Where the distance is reduced by $\Delta d = 0.45\lambda_0$ (caused by the elongation of PZT), and the red peaks are moved to the green ones. In the process of simulation, if $\Delta d = \lambda_0/2$ is adopted, the new peaks will overlap with the red ones. That is to say, when the distance between the mirrors is scanned through a separation corresponding to a phase change of $\Delta\phi = 2 \times 2\pi\Delta d/\lambda_0 = 2\pi$, there will scan by one free spectral range. Where a phase change of 2π happens to be the period of function in Eqs. (1) or (2). Similarly, for confocal FP scanning interferometer as shown in Fig. 3(c) where the light travels 4 times (not 2 times as used in simulation) of distance of two mirrors then interference with the adjacent light. We should note that the distance change of $\Delta d = \lambda_0/4$ will lead to a phase change of $\Delta\phi = 4 \times 2\pi\Delta d/\lambda_0 = 2\pi$ corresponding to the period of function in Eqs. (1) or (2), further to a free spectral range scanning.

For a CW laser (considering the 1064-nm "blue" line shown in Fig. 2), when the transmission spectrum (peak) of the FP is scanned past 1064 nm, the laser light is detected after the FP (narrow filter). For pulsed lasers a saw tooth voltage ramp with frequency much below the laser repetition rate is applied to the piezo. In that case several individual laser pulses will be transmitted during coincidence of FPI transmission band and laser wavelength. From the envelope of these pulses the spectral linewidth of the laser can be estimated. Because of higher pulse peak power, the detected intensity is generally higher in this case than that of the CW laser. This forms the basic idea of the FP scanning interferometer as used in our study.

We remark here on the observance of small transmission peaks ("sub-peaks") on both sides of the maximum peak in the curves corresponding to $m = 10$ (Fig. 1(a)) and $R = 0.98$ (Fig. 1(b)). From Fig. 2,

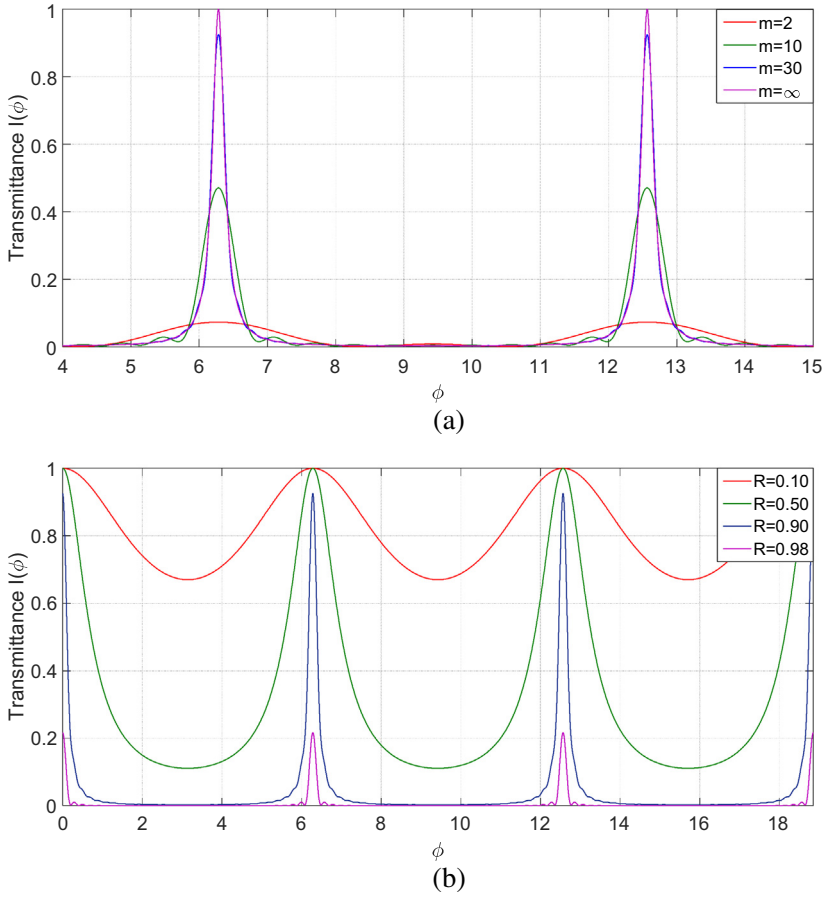

Fig. 1. Relationship between intensity transmittance of the Fabry–Pérot (FP) interferometer and phase difference. (a) $R = 0.90$, and m is varied. (b) $m = 30$, and R is varied.

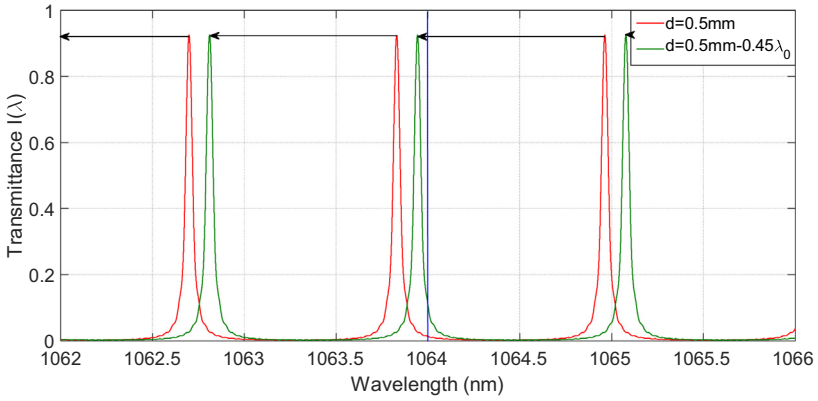

Fig. 2. Principle of Fabry–Pérot (FP) scanning interferometer ($m = 30$, $R = 0.90$, and $\lambda_0 = 1064$ nm). (For interpretation of the references to colour in this figure legend, the reader is referred to the web version of this article.)

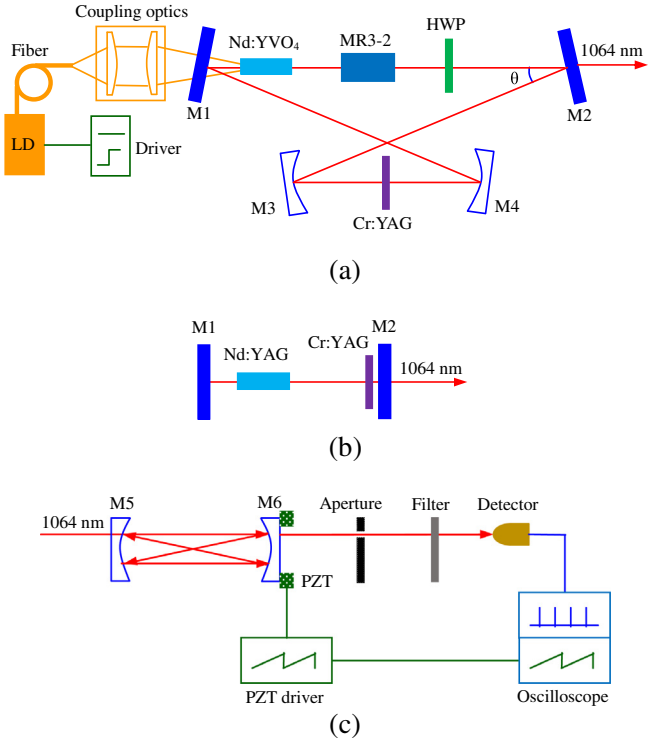

Fig. 3. Experimental setup used in our study. (a) Ring cavity for single-longitudinal-mode operation. (b) Standing-wave cavity for multi-longitudinal-mode detection. (c) Confocal Fabry–Pérot (FP) scanning interferometer.

we note that this situation can be avoided by suitably choosing the FP parameters so that the smaller peaks are not mistaken for a higher-order longitudinal mode corresponding to the laser line.

Experimental setup

The experimental setup used in this study is shown in Fig. 3. The ring cavity parameters in Fig. 3(a) are chosen following a previous study [15]. The optical path length is 530 mm, corresponding to the longitudinal-mode interval of 566 MHz.

In order to detect multi-longitudinal modes, the ring cavity is replaced with a "straight" cavity, as shown in Fig. 3(b). The Nd:YVO_4 crystal is replaced by an identically sized Nd:YAG crystal to achieve stable Q-switched operation. The optical path length is 67 mm, corresponding to the longitudinal mode spacing of 2.24 GHz.

The confocal FP scanning interferometer shown in Fig. 3(c) is used to measure the linewidth obtained with the setup shown in Fig. 3(a). The radius of curvature of the two mirrors is 75 mm (corresponding to the free spectral range of 1 GHz), the intensity reflectivity is 0.90, and the theoretical finesse and resolution are 30 and 35 MHz, respectively.

A flat-flat FP scanning interferometer (not shown) is used to measure the linewidth obtained with the setup in Fig. 3(b). The intensity reflectivity of the mirrors is 0.98, and the free spectral range is 10 GHz, corresponding to theoretical finesse of 156 and resolution of 64 MHz.

From Fig. 2, we note that for the confocal and flat-flat FP scanning interferometers, a cavity length change of 1/2 wavelength will lead to a change of two respectively one free spectral range.

The driver for the PZT shown in Fig. 3(c) can provide a continuously adjustable saw-tooth wave voltage in the frequency range from 0.001 Hz to 100 Hz and voltage range from 0 V to 200 V. At maximum voltage, the maximum displacements of the PZT are 1 μm and 2 μm for the confocal and flat-flat FP scanning interferometers, respectively.

For waveform observation, we use a Tektronix TDS 3032C oscilloscope with a bandwidth of 300 MHz and sampling rate of 2.5 GS/s.

In the experiments, the laser light passing through the FP scanning interferometer is spatially filtered through a small aperture, spectrally filtered from an 880-nm pump light, and subsequently detected by different time response detectors.

Laser linewidth detection by high-speed detector

The Q-switched pulsed laser linewidth has been detected by low speed detector of silicon photocell detector (rise time < 1.2 μs) in our previous work [15]. Further, silicon photocell detector is replaced by a Newport 818-BB-21 high-speed detector (rise time < 200 ps) in this study. The oscilloscope is set to "50-Ω" impedance matching in the "sampling" mode. The test results are shown in Fig. 4(a). Q-switched pulses appear occasionally within the slope of the saw-tooth voltage. We save the data of oscilloscope in the *.CVS file format and find there are a maximum of 10-k sampling points. The saw-tooth scanning period is as long as 100 ms (10 Hz), while the Q-switched pulse width is as short as 40 ns (Fig. 5(d)). The oscilloscope cannot capture short pulses stably when it is set as Fig. 4(a). This may be due to the use of the commercialized FP scanning interferometer to detect the CW laser linewidth, instead of being used to detect the pulsed laser linewidth [10]. Upon assuming that the acquisition of 10 points can be utilized to draw a pulse shape with 40-ns duration, then 50-M

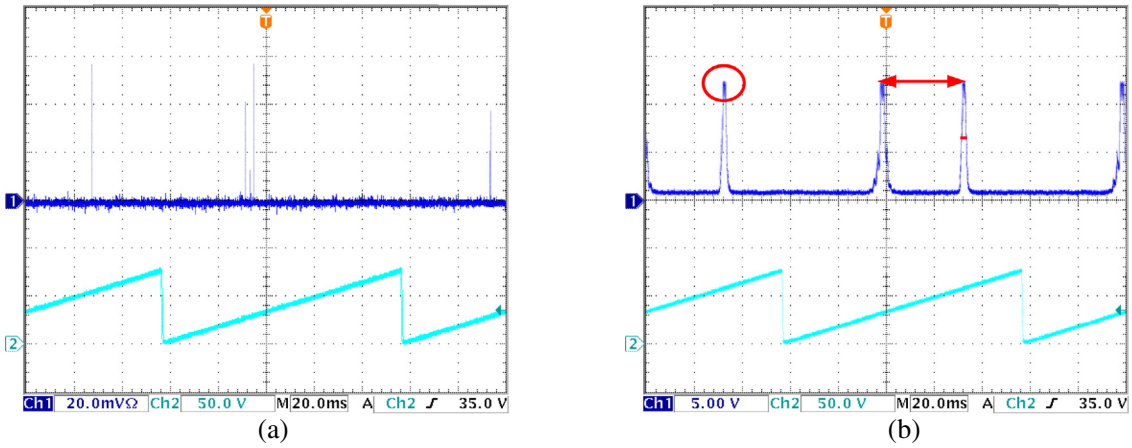

(a) (b)

Fig. 4. Newport 818-BB-21 high-speed detector for detecting linewidth of Q-switched laser. (a) Oscilloscope is set to 50-Ω impedance matching in the sampling mode. (b) Oscilloscope is set to 1-MΩ impedance matching in the sampling mode.

instead of 10-k points are needed. It is unrealistic for current oscilloscope at least.

In the second stage of the experiment, the oscilloscope is set to "1-MΩ" impedance matching in the "sampling" mode as silicon photocell detector. The test results are shown in Fig. 4(b), and they are very similar to those of the CW laser, except for the "modulation depth" being less than 15%.

Next, the oscilloscope is set to "50-Ω" impedance matching in the "peak-detecting" mode; these test results are shown in Fig. 5 (a). The longitudinal mode contour profile exhibits 100% modulation depth and fine structure as described in [15] which is Q-switched pulse train.

The laser in the setup in Fig. 3(a) is next changed to a pulse-pumped laser. The Q-switched pulse repetition rate is the same as that of the pump pulse, which can be varied from 1 Hz to 25 kHz. Fig. 5(b) shows the result with magnification of the horizontal axis of Fig. 5(a), and the result shows several small spikes with a Q-switched pulse repetition rate of 2 kHz. Further magnification of the axis (Fig. 5(c)) shows that the average Q-switched laser pulse width is 40 ns. When the pulse width is measured by

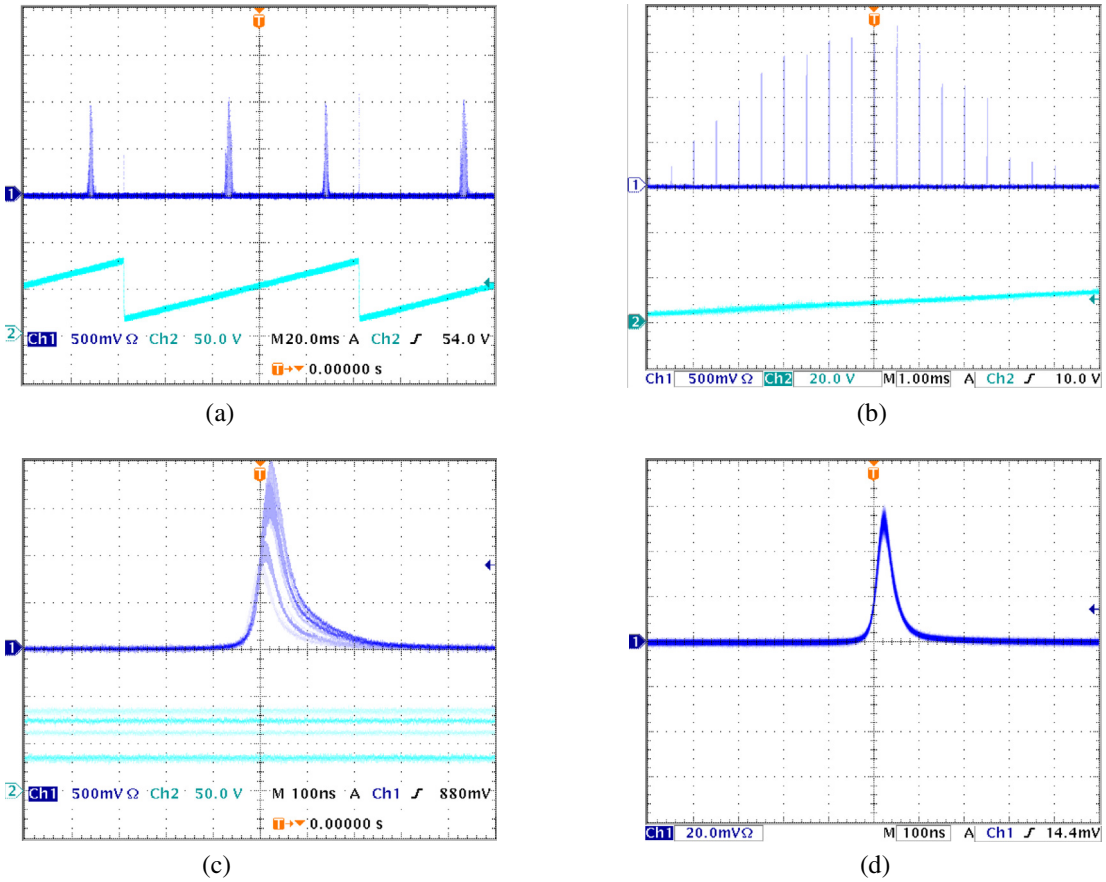

(a) (b)

(c) (d)

Fig. 5. Linewidth and pulse width detection of Q-switched laser with Newport 818-BB-21 high-speed detector. The oscilloscope is set to 50-Ω impedance matching in the "peak-detecting" mode for Fig. 5 (a)–(c), while 50-Ω impedance matching and "sampling" mode for Fig. 5 (d).

the high-speed detector directly, the result is shown in Fig. 5(d). By comparison Fig. 5(c) and (d), it can be seen that the pulse width is not stretched by FP [22]. Meanwhile, the linewidth is about 100 MHz from Fig. 5(a) as shown in Section"*Laser linewidth detection with pulse repetition rate as low as 1 Hz*".

Laser linewidth detection with pulse repetition rate as low as 1 Hz

In the light of the above discussion, we remark here that the output repetition rate of the Q-switched laser can be reduced further with the use of a pulse pump. Further, it can be predicted that at the scanning frequency of 10 Hz, the number of laser pulses will reduce in the longitudinal-mode contour profile. In contrast, the higher is the pulse repetition rate, the more pronounced is the contour profile of the linewidth.

Meanwhile, we note that the calculation of linewidth relies on the proportional relationship between the contour profile of the longitudinal mode and the free spectral range. We use Fig. 4(b) as an example to calculate the single-longitudinal-mode linewidth. The free spectral range and linewidth are red lines, respectively, as shown in Fig. 4(b). And the corresponding relationship for calculating linewidth is shown in Table 1. The scanning frequency does not affect the test results. Thus, in order to increase the number of Q-switched pulses in longitudinal-mode contour profile for a low repetition rate of the laser, the scanning frequency must be further reduced.

In the experiment, the pulse repetition rate of the Q-switched laser is reduced to as low as 1 Hz. The scanning frequency of the saw-tooth wave voltage is correspondingly reduced to 0.01 Hz. The corresponding period is 100 s, which is the maximum time span of the full screen of the oscilloscope used in the study. Fig. 6 shows the test results for this case. In the figure, we observe two Q-switched pulse "clusters" composed of four Q-switched pulses each. Connecting the endpoints of four Q-switched pulses to draw the contour profile yields the linewidth as shown in Fig. 6 (red dashed line). The span of the two pulse clusters corresponds to the free spectral region of 1 GHz, and the longitudinal-mode linewidth is still about 100 MHz according to proportional calculations (similar to Table 1). From this point of view, in order to measure the linewidth of the pulsed laser, we remark that there must be a sufficient number of laser pulses (at least 3) to show the contour profile. If it is required to measure the single pulse linewidth, an FP etalon can be adopted [20].

Multi-longitudinal mode laser linewidth detection

The linewidth measurements for single-longitudinal mode are carried out as described in the previous section. Next, we demonstrate the linewidth measurements for pulsed multi-longitudinal-mode laser (Fig. 3(b)) to validate the proposed method. In order to obtain stable passively Q-switched output for standing cavity, Nd:YVO_4 is replaced by the same size Nd:YAG. Meanwhile, because Nd:YAG yields homogeneous linewidth broadening at room temperature and also because of mode competition, the laser also operates in the single-longitudinal mode, particularly for passive Q-switching. Therefore, we use a shading plate to block the 880-nm pump light, and subsequently remove the plate quickly to capture two longitudinal modes. The results for this case are shown in Fig. 7. The pulse repetition rate and FWHM pulse width are 10 kHz and 14 ns, respectively. The linewidth of one longitudinal mode is estimated to be about 1 GHz.

Table 1
The parameters for calculating linewidth.

	Spectral	Spatial	Temporal
Free spectral range	1 GHz [a]	10 mm [b]	36 ms [c]
Single longitudinal-mode linewidth	Need to be calculated 100 MHz	~1 mm	~3.6 ms

[a] Confocal FP scanning interferometer with radius of curvature of 75 mm.
[b] Gaussian peak fitting using a computer.
[c] Read from time axis of 20 ms/div.

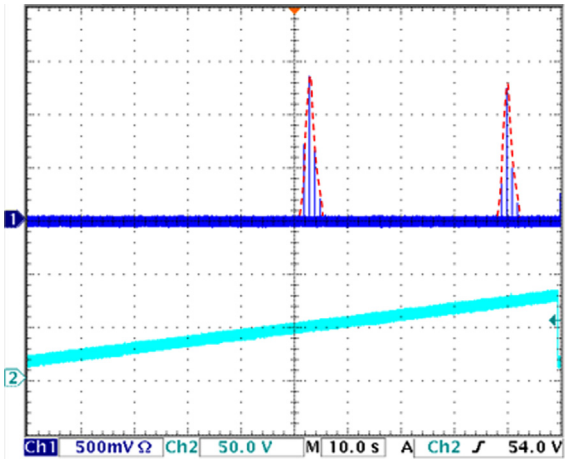

Fig. 6. Linewidth measurement output with pulse repetition rate of 1 Hz and scanning frequency of 0.01 Hz. The Newport 818-BB-21 high-speed detector is used, and the oscilloscope is set to 50-Ω impedance matching in the peak-detecting mode. (For interpretation of the references to colour in this figure legend, the reader is referred to the web version of this article.)

Discussion

Our setup enables single-longitudinal-mode and multi-longitudinal-mode detection with nanosecond pulse widths, as demonstrated in the previous sections. For other pulse durations, due to the limit of the time-bandwidth product (assuming a Gaussian output), the linewidth lies between 150 nm and 1.5 nm for a wavelength of 1.0 μm and pulse duration of 10 fs to 1 ps. For a pulse duration in the range of 1–100 ps, the corresponding linewidth lies between 1.5 nm and 0.015 nm. These pulses linewidths can be detected via a spectrometer with a grating. As regards pulse widths greater than 100 ps, we note that such an output can travel more than 30 mm in the air. Consequently, by carefully selecting the FP scanning interferometer parameters such as the distance between the two mirrors and the reflectivity of the mirrors according to Eq. (1) and Fig. 1, we can ensure that a sufficient number of interference waves will undergo superposition. If the pulse width is too large, the optical path in the air becomes longer than the length of the wave train (coherence length). Consequently, for long pulse, we can design an FP scanning interferometer similar to the one for CW laser.

In the experiment, we also use a Thorlabs DET10C/M detector as the receiving device in the FP scanning interferometer. The parameters of the detectors, oscilloscope settings, and test results are summarized in Table 2. We note that with decrease in the rise time of the detector, the modulation depth gradually decreases with "1-MΩ" impedance matching in the "sampling" mode. The setting of "50-Ω" impedance matching in the "peak-detection" mode is only suitable for high-speed detectors; this setting yields a modulation depth of nearly 100%. The measured linewidth remains the same for a variety of detectors and oscilloscope settings as shown in Fig. 4(b), 5(a), 6 and Fig. 3 in Ref. [15] with the method of Table 1.

During measurement, the nonlinearity and creep effects of PZT are ignored. And at low pulsed repetition rate of the laser, the drifts in temperature or pressure may influence measurement results.

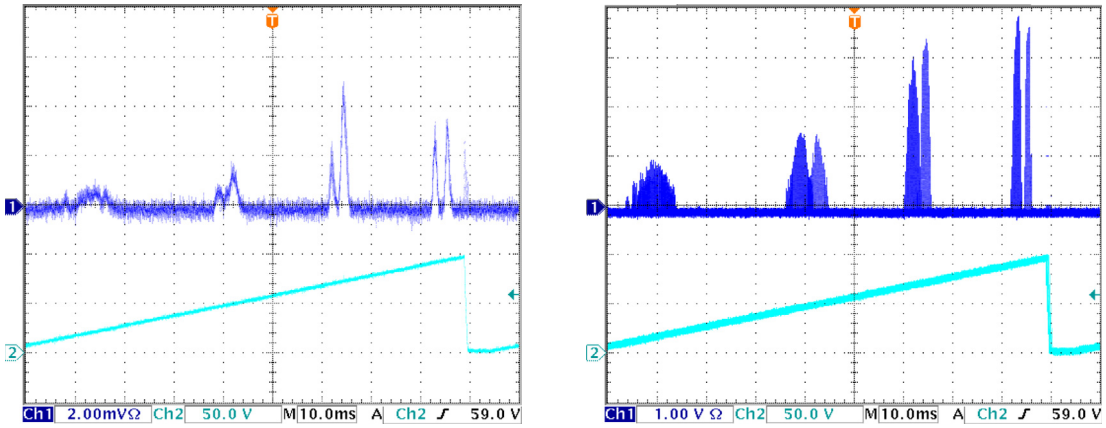

(a) (b)

Fig. 7. Multi-longitudinal mode detection with our setup. The Newport 818-BB-21 high-speed detector is used in this case. The oscilloscope is set to 50-Ω impedance matching in the peak-detecting mode. (a) Detection of two longitudinal modes for CW operation. (b) Detection of two longitudinal modes for passive Q-switching.

Table 2
Test results for different detectors and oscilloscope settings.

No.	Detector	Rise time	Modulation depth[a]	Modulation depth[b]
1 [15]	Silicon photocell	<1.2 μs	~100%	–
2	Thorlabs DET10C/M	<7 ns	<30%	~100%
3	Newport 818-BB-21	<200 ps	<15%	~100%

[a] 1-MΩ impedance matching, sampling mode.
[b] 50-Ω impedance matching, peak-detecting mode.

Conclusion

In this study, we systematically investigated the measurement of pulsed laser linewidths using an FP scanning interferometer. The response of the FP interferometer to continuous and pulsed lasers was analyzed. By carefully choosing the detector along with suitable oscilloscope test parameters, we achieved on-line linewidth measurement of a nanosecond pulsed laser during single-longitudinal-mode and multi-longitudinal-mode operation. We also demonstrated linewidth measurement for as low a frequency as 1 Hz. In addition, we discuss the possibility of detecting linewidths corresponding to pulse widths >100 ps in the 1-μm band. In summary, the application range of the FP scanning interferometer is extended from CW linewidth measurements to pulsed linewidth measurements.

Acknowledgments

We acknowledge support from the Guangdong Province Higher Outstanding Young Teachers Training Program (No. Yq2013208), Guangdong Province Innovative Talent Training Plan of Natural Science Nursery Engineering (No. 2013LYM_0101), and the Eighth "Thousand-Hundred-Ten" Training Targets of Guangdong Province Department of Education.

Appendix A. Supplementary data

Supplementary data associated with this article can be found, in the online version, at http://dx.doi.org/10.1016/j.rinp.2016.10.004.

References

[1] Van Deventer MO, Spano P, Nielsen SK. Comparison of DFB laser linewidth measurement techniques results from COST 215 round robin. Electron Lett 1990;26(24):2018–20.
[2] Beyer T, Braun M, Hartwig S, Lambrecht A. Linewidth measurement of free-running, pulsed, distributed feedback quantum cascade lasers. J Appl Phys 2004;95(9):4551–4.
[3] Okoshi T, Kikuchi K, Nakayama A. Novel method for high resolution measurement of laser output spectrum. Electron Lett 1980;16(16):630–1.
[4] Hsu K, Miller CM, Miller JW. Speed-of-light effects in high-resolution long-cavity fiber Fabry-Perot scanning interferometers. Opt Lett 1993;18(3):235–7.
[5] Hercher M. The spherical mirror Fabry-Perot interferometer. Appl Opt 1968;7(5):951–66.
[6] Johnson JR. A high resolution scanning confocal interferometer. Appl Opt 1968;7(6):1061–72.
[7] Barr WL, Gardner AL. A scanning Fabry-Perot interferometer. J Opt Soc Am 1961;51(12):1400–1.
[8] Huang J, Ma Y, Zhou B, Li H, Yu Y, Liang K. Processing method of spectral measurement using FP etalon and ICCD. Opt Express 2012;20(17):18568–78.
[9] Vorobiev N, Glebov L, Smirnov V. Single-frequency-mode Q-switched Nd:YAG and Er:glass lasers controlled by volume Bragg gratings. Opt Express 2008;16(12):9199–204.
[10] http://www.thorlabs.us/.
[11] Steinmetz LL, Bookless WA, Richardson JH. Recent pulse width and linewidth measurements on the mode-locked Kr+-ion laser. Appl Opt 1980;19(16):2663–5.
[12] Gu G-Q, Zhou F, Zhang G, Chin MK. Passive Q-switched single-frequency Nd:YVO_4 laser with GaAs saturable absorber. Electron Lett 1998;34(6):564–5.
[13] Shen D-Y, Tam S-C, Lam Y-L, Kobayashi T. Diode-pumped passively Q-switched single-frequency Nd:YAG lasers. Opt Rev 2000;7(5):451–4.
[14] Koch P, Bartschke J, L'huillier JA. High-power actively Q-switched single-mode 1342 nm Nd:YVO_4 ring laser, injection-locked by a cw single-frequency microchip laser. Opt Express 2015;23(24):31357–66.
[15] Junwen X, Ying P, Wei C, Yujie F, Haijun X, Mingyuan X. Sun Lu, and S. Binghua, Cr:YAG passively Q-switched single-frequency Nd:YVO_4 ring cavity laser. J Opt Soc Am B 2016;33(9):1815–9.
[16] Monzón JJ, Sánchez-Soto LL. Reflected fringes in a Fabry-Perot interferometer with absorbing coatings. J Opt Soc Am A 1995;12(1):132–6.
[17] Monzón JJ, Sánchez-Soto LL, Bernabeu E. Influence of coating thickness on the performance of a Fabry-Perot interferometer. Appl Opt 1991;30(28):4126–32.
[18] Marzenell S, Beigang R, Wallenstein R. Limitations and guidelines for measuring the spectral width of ultrashort light pulses with a scanning Fabry-Pérot interferometer. Appl Phys B 2000;71(2):185–91.
[19] Born Max, Wolf Emil. Principles of Optics: Electromagnetic Theory of Propagation, Interference and Diffraction of Light. Cambridge University Press; 1999. Chap. VII.
[20] Johnson JB, Johnson MJ, Lyon K. Limitations and guidelines for measuring the spectral width of a single pulse of light with a Fabry-Perot interferometer. Appl Opt 2011;50(3):347–55.
[21] Roychoudhuri C. Response of Fabry-Perot interferometers to light pulses of very short duration. J Opt Soc Am A 1975;65(12):1418–26.
[22] Offrein BJ, Hoekstra HJWM, Van Loenen JP, Driessen A, Popma ThJA. Response measurements of a Fabry-Perot to short pulses. Opt Commun 1994;112(5):253–7.